Defect and Diffusion Forum Vols. 129-130 (1996) pp. 229-242

Diffusion Induced Stresses as a Driving Force for the Instability of a Solid/Liquid Interface

E. Rabkin, B. Straumal and W. Gust

Institut für Metallkunde der Universität and Max-Planck-Institut für Metallforschung, Seestr. 75, D-70174 Stuttgart, Germany

Keywords: Solid/Liquid Interface, Dissolution, Coherency Strain, Dislocation

Abstract—The dissolution of a solid metal in the melt of a metal with a lower melting temperature has been investigated for the case of Fe(Si) monocrystals dissolving in liquid Sn or Zn. The liquid metal penetrates into the monocrystal with an unusually high velocity by inclusions which are isolated from each other. This velocity is at least an order of magnitude higher than it follows from the volume diffusion equation. The inclusions are stretched along specific directions tilted to the solid/liquid interface. Electron probe microanalysis of the compositional distribution in the penetration zone has been performed. The phenomenon has been interpreted as a dissolution process along the dislocation lines promoted by the coherency strain. The thermodynamic conditions for the instability development are given.

1. INTRODUCTION

Rhee and Yoon [1] have revealed the instability of an solid/liquid interface in the Mo–Ni system. In their experiments, the instability of the interface in the form of an indulating structure has been observed in a sintered Mo–15 wt.% Ni alloy heat treated at a temperature of 1400°C which is different from the sintering temperature. The phenomenon has been interpreted in terms of the coherency strain theory [2]: a deviation of the composition of the liquid from the equilibrium value of the annealing temperature leads to a diffusion of solute atoms from the melt into the grain interior. Those regions of the grain surface where the coherency is preserved dissolve, whereas in regions where the coherency is lost a deposition of the solid alloy from the melt occurs. Coherency strains induced by solute diffusion into the solidifying alloy were shown to be the reason for the instability of the solid/liquid interface during the directional solidification [3]. In the present work, we have also found an instability of the solid/liquid interface in the Fe(Si)–Sn and Fe(Si)–Zn systems, however, the morphology of this instability is totally different from the morphology observed [1] and theoretically predicted [3] earlier. The obtained morphologies resemble strongly the well-known Liesegang phenomenon [4] of the nucleation of pores inside a sample during internal oxidation. However, numerical estimations show that the Liesegang mechanism cannot explain the observed instability in our case. We have put forward the hypothesis of the metal dissolution along the dislocation lines, caused by the coherency strain energy. This hypothesis is consistent with the experimental observations.

2. EXPERIMENTAL

Fe–Si alloys with 7 and 12 at.% Si were produced from Fe of 99.99 wt.% purity and Si of 99.999 wt.% purity. Polycrystalline rods were used to grow cylindrical <001> single crystals by the electron beam zone floating technique. Samples 1.5x2x3 mm in size were then cut from the as-grown single crystals. After cutting, the samples were mechanically and chemically polished. Sn and Zn layers of 99.999 wt.% purity were then applied to the samples by immersion into the melt under such conditions that the thickness of the Sn or Zn layer after immersion was about 1 mm.

Preliminary experiments showed that if the thickness of the applied Sn or Zn layer is below approx. 100 μm the instability in which we are interested does not develop. The samples were evacuated in silica ampoules under high vacuum ($4x10^{-4}$ Pa) and heat treated at 964 and 974°C for Fe(Si)–Sn and Fe(Si)–Zn systems, respectively. The temperature of the ampoule increased from room temperature to the desired value within about 10 min, after which it was held constant. After annealing, the ampoules were quenched into water, and the sample were prepared for light microscopy (**LM**) and electron probe microanalysis (**EPMA**) by standard methods. The EPMA measurements were carried out by wavelength dispersive analysis on a JEOL 6400 electron probe microanalyzer operated at 15 kV. The intensities of the FeK_α, SnL_α, and SiK_α peaks were determined, and the concentrations of these elements were obtained utilizing a program in which corrections are considered due to the atomic number, absorption, fluorescence and background.

3. RESULTS

In Fig. 1, the (001) cross-section of an Fe-7 at.% Si sample annealed with liquid Sn is shown after slight etching in a 5% HNO_3 solution. The sample was held in a furnace with a temperature of 964 °C for 20 min. The direction of Sn penetration is <001>. Above the interface between the Fe-based solid solution and the tin there is an approximately 50 μm wide zone of dark inclusions. The average size of the inclusions as well as the distance between the inclusions increase with the distance from the boundary. The inclusions are stretched along a direction which forms an angle of about 45°±2° with the solid/liquid interface. In Fig. 2, the cross-section of an Fe-12 at.% Si monocrystal annealed with liquid Zn at 974°C for 7 hours is shown after etching. The direction of diffusion from the two opposite interfaces is again <001>, but the cross-section plane is now tilted on an angle of 38°±3° around the <010> direction. Again, the zone with inclusions approximately 400 μm in width can be clearly seen. The inclusions are grouped in strings lying in directions forming angles of 37°±2° and 61°±2° with the solid/liquid interfaces. In Fig. 3, the Fe(Si)–Sn

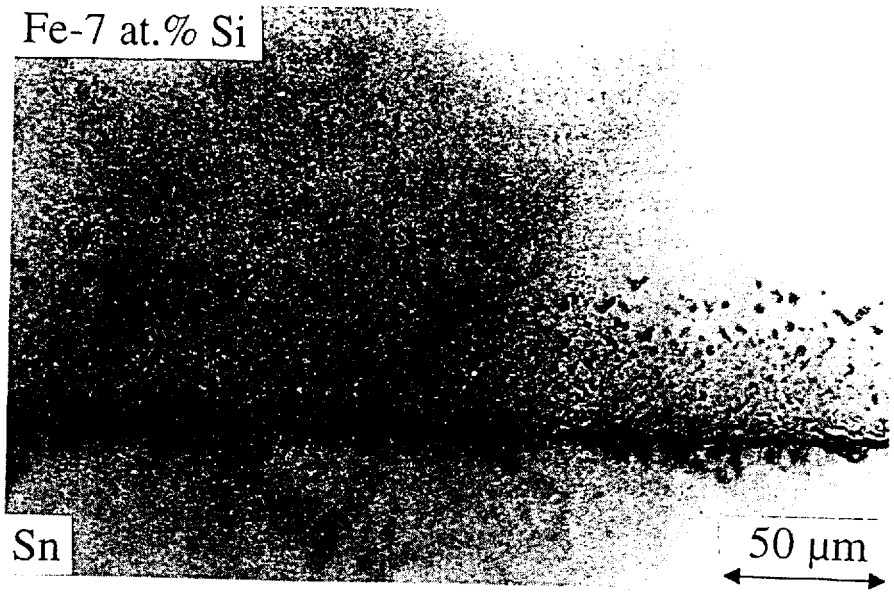

Fig. 1. An optical micrograph of the Fe–7 at.% Si monocrystal annealed in contact with liquid Sn at 964°C for 20 min. The cross-section plane and the plane of the solid/liquid interface are (010) and (001), respectively.

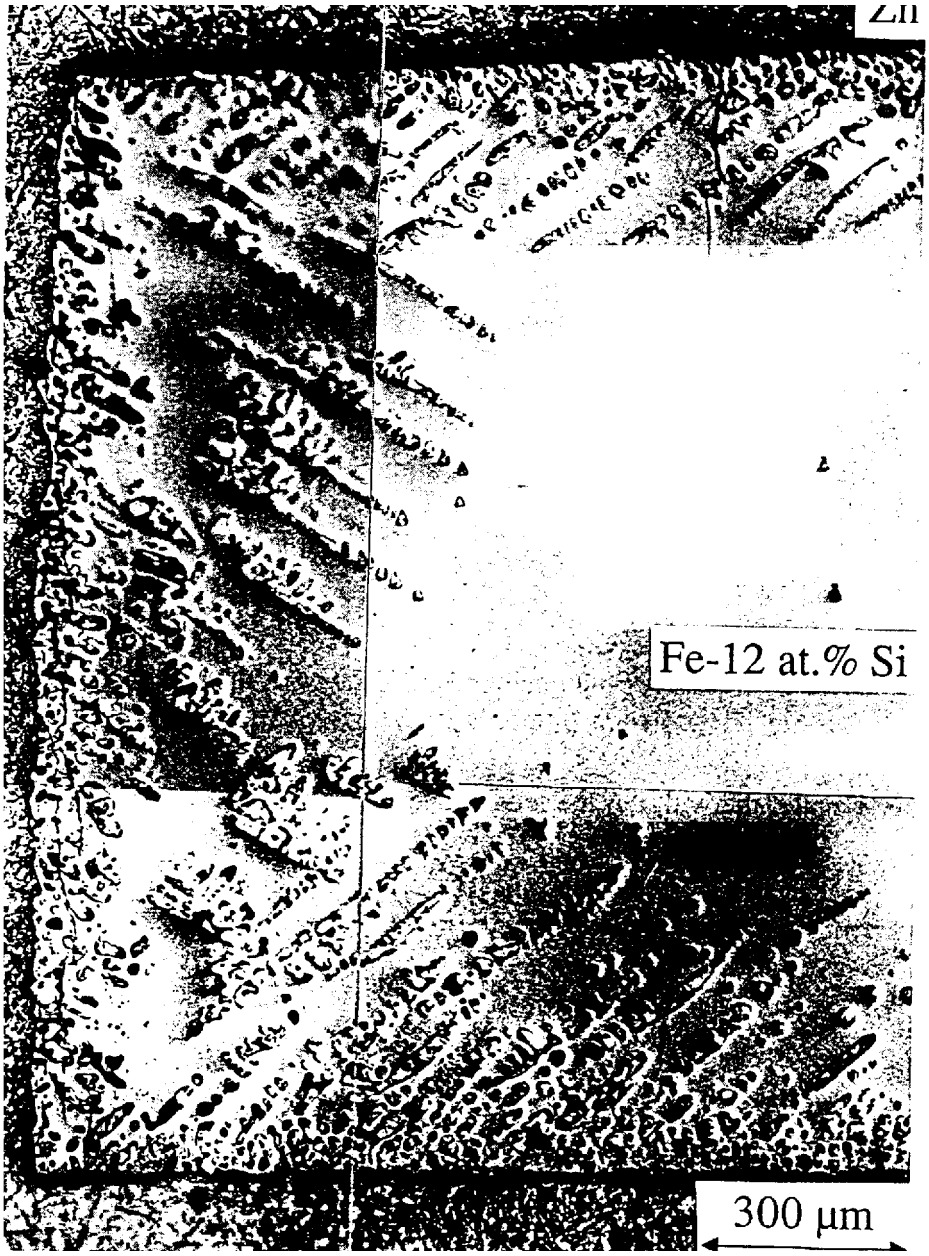

Fig. 2. An optical micrograph of the Fe–12 at.% Si monocrystal annealed in contact with liquid Zn at 974°C for 7 h. The planes of horizontal solid/liquid interfaces are (001), but the cross-section plane is rotated around <001> by an angle of 38°.

sample with its structural features is drawn schematically, and the segments where the EPMA measurements were made, are shown. In Fig. 4 the concentration profiles of Fe, Sn and Si are shown in the solidified Sn-rich melt (1–1'), in the zone of inclusions parallel to the solid/liquid interface near it (2–2') and far from it (3–3'), and perpendicular to the interface (4–4'). The results of the EPMA measurements allow us to identify the inclusions with the Sn-rich phase, which penetrated in such an unusual way into the monocrystal during the anneal. One cannot determine the exact Sn concentration in the inclusions because the size of the excitation zone of the electron beam during EPMA is comparable with the size of an inclusion. The best estimation of the composition inside the inclusion should therefore be taken from the EPMA values for the widest inclusion.

Obviously, this is for the first peak in Fig. 4(c) where approximately 16.5 at.% Fe, 82 at.% Sn and 1.5 at. % Si are present. The concentration of Si in the melt [see Fig. 4(a)] is also 1.5±0.2 at.%. This is a strong evidence that the Sn-rich phase inside the inclusions was liquid during the anneal. The composition in the middle of the particle in Fig. 4(a) is about 50 at.% Sn and 50 at.% Fe, which corresponds to the intermetallic phase FeSn which is stable up to 770 °C. Probably, this phase formed during the quenching. No further intermetallic phases in the solidified Sn melt were found, which is an indication of a high cooling rate. A comparison of Figs. 4(b) and 4(a) confirms the LM observation that the inclusions in the vicinity of the interface are smaller than far from it. The Si concentration in the Fe-based solid solution in the vicinity of the solid/liquid interface (both at the surface of the sample and near the inclusions) is about 1 at.% higher than the initial concentration of 7 at.%. This is due to the dissolution process of the Fe-based solid solution in the Sn-rich melt. As the solubility of Si in the melt does not exceed 1.5–1.6 at.% Si, the excess of Si is forming in the solid solution near the interface during the rapid dissolution process. The Sn concentration in the solid solution between the inclusions decreases continuously with the distance from the interface [Fig. 4(d)] from approx. 2 at.% near the interface to 1.6 at.% between two last inclusions.

DISCUSSION AND MODEL

The microstructures which we observed (see Figs. 1 and 2) resemble strongly the microstructures caused by the Liesegang phenomenon. However, the following reasons exclude the mechanism of Liesegang phenomenon proposed by Wagner [5] as a possible explanation of our experiments.

- According to Wagner, the width of the precipitation zone is proportional to $\sqrt{Dt}$ where D is the

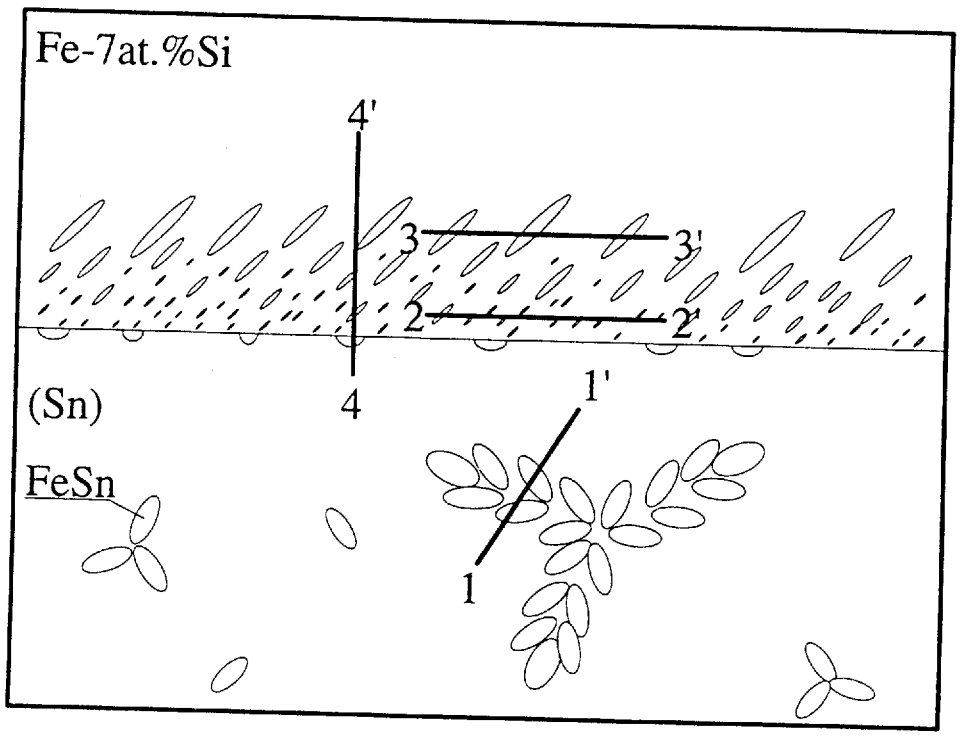

Fig. 3. Schematic diagram of the microstructure of an Fe–7 at.% Si monocrystal after interaction with the liquid Sn. The segments, where the EPMA measurements were made, are shown.

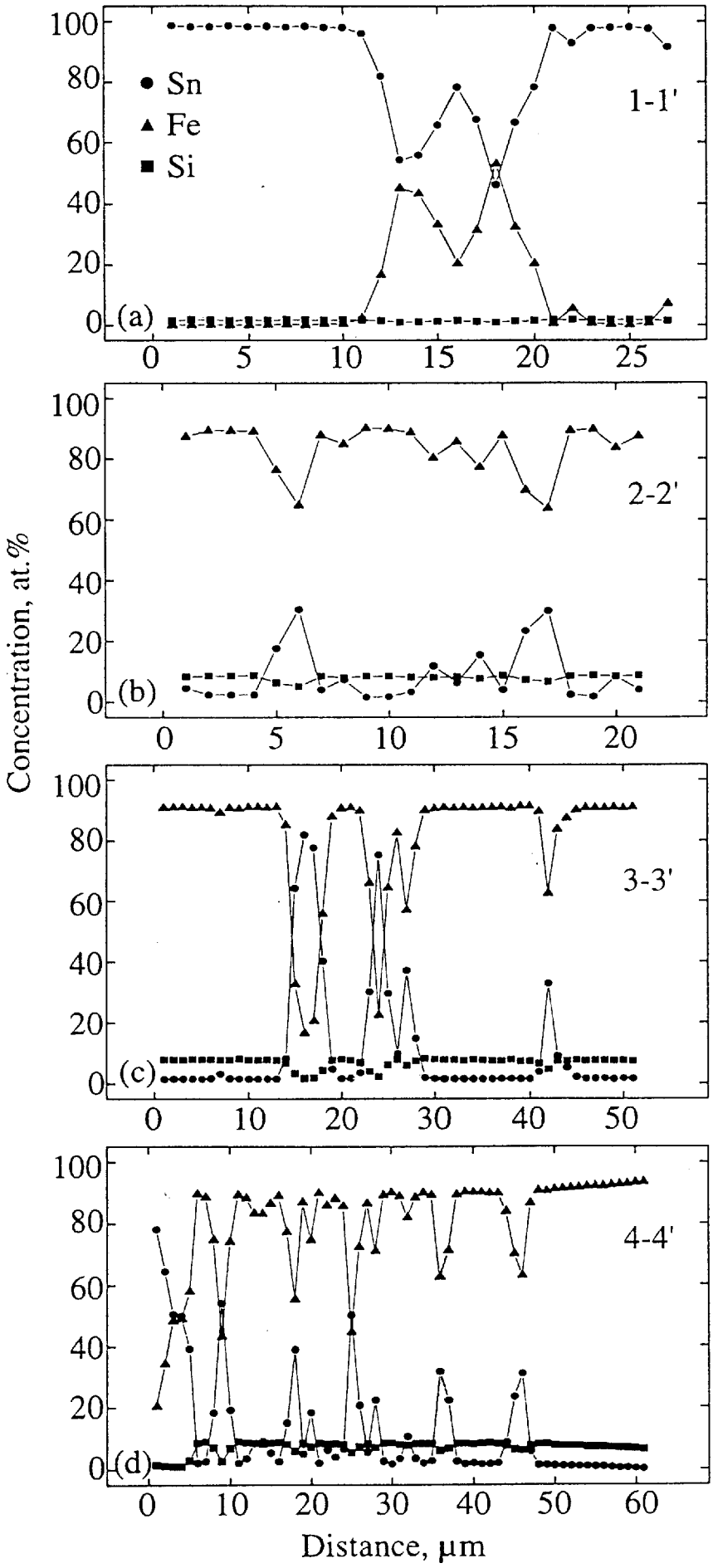

Fig. 4. **(a-d).** The EPMA measurements of the element distribution along the trajectories shown in Fig. 3.

volume diffusion coefficient, which was assumed to be the same for both species in the binary system, and t is the annealing time. Obviously, the highest value of the diffusion coefficient should be accepted for estimations. The interdiffusion coefficient of Sn and Zn in Fe–5 at.% Si has been measured [6]. Recently, we have measured the interdiffusion coefficients in the Fe–Si system in the concentration interval 6–18 at.% Si [7]. Using the Arrhenius parameters from these works one can estimate the interdiffusion coefficients for 964°C (D_{Sn}=1.2x10^{-13} m^2/s and D_{Si}=1.7x10^{-13} m^2/s) and 974°C (D_{Zn}=1.5x10^{-13} m^2/s and D_{Si}=2.1x10^{-13} m^2/s). For the 10 min anneal at 964°C this corresponds to an average size of the zone with precipitates of about 10 μm, which is by a factor of 5 lower than the observed width of the zone with inclusions (about 50 μm, see Fig. 1). For the Fe(Si)–Zn sample annealed at 974°C for 7 h, $\sqrt{D_{Si}t} \approx 73$ μm which again is by a factor of 5 lower than the observed width of the zone with the precipitates (about 400 μm, see Fig. 2).

• The ordered arrangement of the inclusions organized in bands tilted on a definite angle with respect to the direction of diffusion has been never observed in the Liesegang phenomenon, even in experiments with Ag monocrystals [8]. Normally, the pores are arranged in bands which are parallel to the diffusion front, which is connected with the isotropy of the diffusion coefficient in cubic crystals. The geometry of precipitates in our case can be understood if one assume that they are arranged along the lines lying in the (011) planes. These planes will give the intersection lines on the (001) cross-section tilted on 45° to the solid/liquid interface. For the tilted cross-section the intersection lines should be tilted on 38.2° and 58.4°, which is in good agreement with the observations.

It is clear from the above said that some mechanism different from the bulk interdiffusion should be involved in the formation of precipitates inside the solid. We think that the *dissolution of a solid in the melt along the dislocation lines* is the mechanism responsible for the observed morphologies. The groups of dislocations in the (011) planes, which are the characteristic slip planes for body-centred cubic metals, will give the observed arrangement of inclusions. Frank [9] considered the possibility of the existence of open-cored dislocations. The balance between the surface and elastic stress energies for screw dislocations with a hollow core of a radius R gives the following expression for the equilibrium value of the radius [9]:

$$R_{Frank} = \frac{Gb^2}{8\pi^2\gamma_s} \tag{1}$$

where G, b and γ_s are the rigidity modulus, the Burgers vector of the dislocation and the excess surface energy (surface tension) of the metal, respectively. For parameter values typical for metals the R value calculated according equation (1) is less than 1 Å, and the open-cored dislocations do not exist. However, if we consider the dislocation core filled with a liquid meal, the γ_s value in equation (1) should be substituted by the surface tension γ_{SL} of the solid/liquid interface, which is normally much lower than γ_s. For example, for Fe $\gamma_s \approx 2320$ mJ/m^2 (1410°C, H_2 atmosphere), whereas for Fe–Cu at 1125 °C $\gamma_{SL} \approx 400$ mJ/m^2 [10]. Therefore, for the dislocation core filled with a liquid metal the consideration of Frank can be relevant. Moreover, for systems like Fe–Sn or Fe–Zn where a considerable solubility of the second metal in Fe exists, the energy of coherency strains should be taken into account. The process of dissolution of the dislocation core is controlled by the rapid diffusion in the liquid phase. It means that the width of the zone of volume diffusion out of the dislocation core can be small enough for keeping the coherent relationship with the matrix without atoms of the diffusant. Below, a detailed analysis of the stability of a dislocation with a cylindrical core filled with a liquid metal will be given.

Let us consider the following model. In the core of a screw dislocation in Fe a cylinder of liquid Sn is present (Fig. 5). Sn atoms diffuse from that cylinder into the solid. Because the diffusion rate in a liquid is much faster than in a solid, the stability of such a dislocation is determined by the equilibrium composition of the Sn-rich melt inside the cylinder. This composition is different from the composition of the bulk melt near the solid/liquid interface due to three reasons: (i) the capillarity effect; (ii) the energy of elastic stress induced by the screw dislocation and (iii) the coherency strain energy of the diffusion zone near the dislocation. We suppose that the coherency of the diffusion zone at the original solid/liquid interface is lost in the first seconds of the anneal, because the dissolution rate from this interface is rather slow (the linear dimensions of the sample in Fig. 2 are close to those before anneal) and the characteristic size of the diffusion zone at which the coherency is normally lost (about 100 Å) can be reached in this short time. If the difference in Sn concentration Δc_L inside the cylinder and in the bulk melt (equilibrium liquidus concentration c_L) is negative, then Sn will be supplied to the dislocation core from the bulk melt and at the same time Fe atoms will diffuse from the core region into the bulk melt. The dislocation will be unstable against the dissolution. We should therefore calculate the concentration difference Δc_L. The following simplifying assumptions will be made for the calculations: (1) The binary Fe–Sn system will be considered instead of the ternary Fe–Sn–Si one; (2) The Fe-based solid solution and the Sn-rich liquid alloy will be described by the regular solution model; (3) The solid solution will be described as an elastically isotropic medium. The simplifications made are not of principal importance and the result obtained can be easily generalized in these respects. The condition of thermodynamic equilibrium between the uncurved and unstressed solid and the melt can be written in the form:

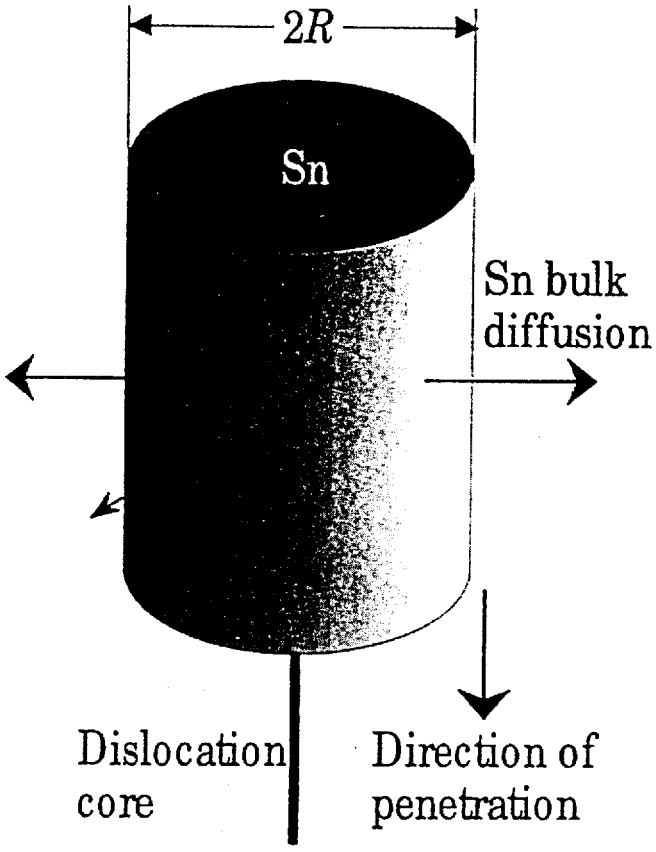

Fig. 5. The model: the Sn-rich liquid alloy dissolves the matrix metal and penetrates along the dislocation line. Due to the bulk diffusion of Sn atoms into the matrix the coherently strained layer of an alloy is formed.

$$\mu_{0S}^{Sn} + RT\ln c_S + \Omega_S(1-c_S)^2 = \mu_{0L}^{Sn} + RT\ln c_L + \Omega_L(1-c_L)^2$$
$$\mu_{0S}^{Fe} + RT\ln(1-c_S) + \Omega_S c_S^2 = \mu_{0L}^{Fe} + RT\ln(1-c_L) + \Omega_L c_L^2 \quad (2)$$

where c_S, Ω_S, Ω_L, μ_0, R and T are the Sn solidus concentration, the interaction parameters from the regular solution theory for the solid and liquid phases, the standard value of the chemical potential, the gas constant and the absolute temperature, respectively. On the inner surface of the cylinder, however, the energy of Fe and Sn atoms in the solid are different from those at the uncurved and unstressed surface. For the density of the coherency strain energy, E_{coh}, the expression for a coherently strained half-space can be used

$$E_{coh} = \frac{E\eta^2 c_S^2}{1-\nu} \quad (3)$$

where $\eta = d\ln a/dc$, a being the lattice parameter of the alloy with the concentration c, and E and ν are the Young's modulus and Poisson's ratio, respectively. The expression (3) is valid for the density of the coherency strain energy for the atoms on the arbitrary curved surface. The reason is that the normal stress at the surface should be equal to zero (or to the hydrostatic pressure p in the liquid, but we assume $p=0$) in order to satisfy the condition of the mechanical equilibrium of the surface. Therefore, the coherency strains are $-\eta c$ in two perpendicular directions of the tangential to the surface plane, which makes the problem equivalent to the problem of a coherently strained half-space. In the Appendix, the mathematical proof of this statement is given for a hollow cylinder. Strictly speaking, in a solid under stress other than a hydrostatic one the chemical potentials of atoms have no physical meaning [11]. However, it can be shown that for an elastically isotropic substitutional solid solution in contact with a liquid alloy where the hydrostatic pressure $p=0$ the conditions of thermodynamic equilibrium of Larché and Cahn [12] can be written in such a form which one can get calculating the "apparent" chemical potentials from the elastic energy given by equation (3) using the standard thermodynamic equations. We will use further such a "chemical potential" method because it is more obvious than the others. The total change of the chemical potentials of Fe and Sn atoms in the solid at the cylindrical interface is simply the sum of three contributions because the tangential strain caused by the screw dislocation does not interact with the normal coherency strain:

$$\Delta\mu_{Sn} = V_m\left\{\frac{Gb^2}{8\pi^2R^2} + \frac{E\eta^2 c_S(2-c_S)}{1-\nu} - \frac{\gamma_{SL}}{R}\right\}$$
$$\Delta\mu_{Fe} = V_m\left\{\frac{Gb^2}{8\pi^2R^2} - \frac{E\eta^2 c_S^2}{1-\nu} - \frac{\gamma_{SL}}{R}\right\} \quad (4)$$

where V_m is the molar volume, which is assumed to be the same for the Fe and Sn atoms. We also neglect the change of V_m induced by stress (this will give corrections of the second order) and the concentration dependence of the elastic constants. Substituting equations (4) into (2) and taking into account only the terms of the first order on Δc_L and Δc_S where Δc_S is the change of the solidus concentration, one can calculate Δc_L:

$$\Delta c_L = \frac{c_L(1-c_L)V_m}{(c_L-c_S)\left[RT-2\Omega_L c_L(1-c_L)\right]}\left\{\frac{\gamma_{SL}}{R}-\frac{E\eta^2 c_S^2}{1-\nu}-\frac{Gb^2}{8\pi^2R^2}\right\} \tag{5}$$

The cylinder filled with the melt is in equilibrium with the bulk melt if $\Delta c_L=0$. From equation (5), taking into account that for an isotropic medium $G = E/2(1+\nu)$, we get for the equilibrium radius

$$R = R_{Frank}\frac{2}{1\pm\sqrt{1-\left(\frac{E\eta c_S b}{2\pi\gamma_{SL}\sqrt{1-\nu^2}}\right)^2}} \tag{6}$$

We see that now there are two solutions, the first one with the plus sign in the denominator being stable and the second one with the minus sign being unstable against dissolution. For

$$\gamma_{SL} \le \gamma^*_{SL} = \frac{E\eta c_S b}{2\pi\sqrt{1-\nu^2}} \tag{7}$$

$\Delta c_L(R) < 0$ for all values of R, and the dislocation is *absolutely unstable* against dissolution in the liquid Sn. All above said is illustrated in Fig. 6, where the dependence $\Delta c_L(R)$ is calculated by using the following values for the Fe–Sn system (E=2.11x10^{11} Pa, ν=0.293, η=0.23, c_S=0.1, c_L=0.93, b=2.48x10^{-10} m, $\Omega_L \approx$ 29.550 kJ/mol and V_m=7.1x10^{-6} m^3/mol [13]) and by using two

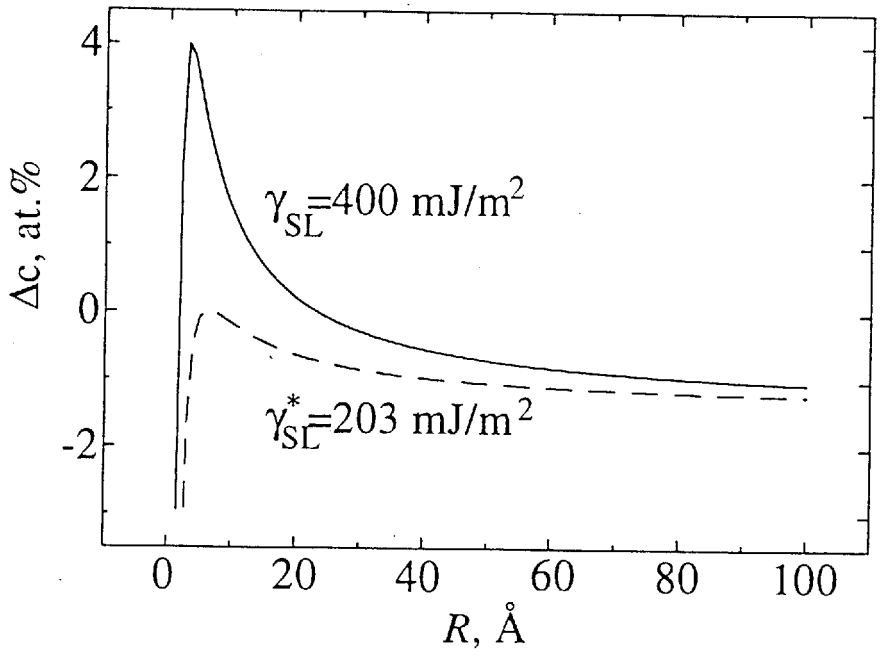

Fig. 6. The dependence of the Sn supersaturation Δc in the cylinder of a Sn-rich liquid alloy along the dislocation core on the radius R of the cylinder for two values of γ_{SL}.

values of γ_{SL}: γ_{SL}=400 mJ/m^2 and $\gamma_{SL} = \gamma^*_{SL} \approx 203$ mJ/m^2. One can see that even at high values of γ_{SL} the dislocation is unstable against dissolution at high R values, however, the supersaturation barrier should be overcome in this case. Here, the role of the undersaturation of the original melt can be understood. If the bulk melt is undersaturated to such an extent that the maximum on the $\Delta c_L(R)$ dependence gives a Sn concentration at the tip of the dissolving dislocation still below the Sn concentration in the Sn-rich melt, the dissolution process will progress. In our consideration we have not considered the possible widening of the cylinder filled with the melt near the bulk solid/liquid interface (dislocation etching pit). Srolovitz and Safran [14] have shown that the formation of deep elongated pits is possible, implying that the open core dislocations can exist even for $R > R_{Frank}$. Therefore, one can conclude that this effect promotes the considered instability.

The interesting question about the kinetics of the dissolution process along the dislocation cores and the evolution of the morphology with time lye beyond the scope of the present paper. We should only note that normally there are too many dislocations in a crystal so that all of them cannot be wetted by the liquid phase. Even if it is the case at the beginning of the dissolution process, then the condition for the A-regime of the diffusion along dislocation pipes ($\sqrt{Dt} > 10d$ where d is the average distance between the dislocations [15]) will be fulfilled quickly, because d is normally very small. In the A-regime the diffusing atoms are homogeneously distributed in the solid, therefore, there will not be any coherency strain available (for a coherently strained diffusion zone the presence of a large region of pure matrix without solute atoms is necessary). Therefore, for the operation of the proposed mechanism of the coherency strain-assisted dissolution the condition $d^* \gg 0.1\sqrt{Dt}$ should be valid, where d^* is the distance between the dislocations which are dissolving. From Figs 1 and 2 it can be seen that the distance between the inclusion bands corresponds approximately to $\sqrt{Dt}$. Furthermore, at the regions of the dislocation line close to the original solid/liquid interface the width of the bulk diffusion zone around the dislocation is higher than deep inside the specimen. The coherency can be lost there and the driving force for dissolution disappear. The radius R of the liquid cylinder will slowly decrease there under the action of the surface tension and bulk diffusion. Indeed, it can be seen from Figs 1 and 2 that inclusions deep in the sample are larger than those close to the original solid/liquid interface.

It should be noted that the proposed consideration could be applied to a wide variety of phenomena of interaction between solid and liquid metals. For example, it follows from equation (5) that the cracking of a solid metal in a melt is possible without any external stress: the radius R in this case is the radius of curvature of the tip of the growing crack, and if the growth rate of the crack is high enough for the coherency at the tip to be preserved, then an equation similar to equation (5) is valid, but including only the first two terms in the braces. All cracks with the tip radius higher than

$$R_{crit} = \frac{\gamma_{SL}(1-\nu)}{E\eta^2 c_S^2} \tag{8}$$

will grow. For the Fe–Sn system with γ_{SL}=400 mJ/m^2 we get the reasonable value $R_{crit} \approx 25$ Å.

Another example is the mysteriously rapid penetration of liquid Ga along grain boundaries (GBs) in Al [16]. The problem here is that there is no remarkable difference in the physical properties of Ga with respect to other metals with a low melting point like Zn, Sn, In or Hg, penetration rates of which along GBs in Al are orders of magnitude lower than for Ga. Again, taking into account the coherency strain energy clarifies the situation. Let us consider the tip of the GB groove filled with a liquid metal (Fig. 7). We also consider the GB region as a separate "GB phase"

for which the chemical potentials of atoms μ_{GB} can be defined. In the GB phase the tensile stress of the amplitude γ_{GB} is operating where γ_{GB} is the excess energy of the GB. Therefore, the condition of full equilibrium is

$$\mu_{GB} - \gamma_{GB} A = \mu_S^e \tag{9}$$

where A and μ_S^e are the molar area of the alloy and the equilibrium chemical potential of atoms in the solid solution, respectively. The atom at the tip of the GB groove (solid circle in Fig. 7) is subjected to the tensile stress of the amplitude $2\gamma_{SL}$ only, if $2\gamma_{SL} < \gamma_{GB}$., and the chemical potential of atoms in the solid solution near the groove will differ from its equilibrium value:

$$\mu_{GB} - 2\gamma_{SL} A = \mu_S. \tag{10}$$

Subtracting equation (9) from (10) we get

$$\Delta\mu_S = (\gamma_{GB} - 2\gamma_{SL})A. \tag{11}$$

An analysis similar to that one used for equations (4) and (5) gives for the supersaturation of the liquid alloy at the tip of the GB groove

$$\Delta c_L = -\frac{c_L(1-c_L)}{(c_L - c_S)\left[RT - 2\Omega_L c_L(1-c_L)\right]}\left\{(\gamma_{GB} - 2\gamma_{SL})A + \frac{V_m E \eta^2 c_S^2}{1-\nu}\right\}. \tag{12}$$

Recently, Fradkov [17] has shown that for the formation of deep narrow grooves along GBs an undersaturation of the melt with the atoms of the crystal matrix is needed. Equation (12) demonstrates that for the positive spreading $\gamma_{GB} - 2\gamma_{SL}$ such an undersaturation always exists even for the bulk melt equilibrated with the bulk crystal. Numerical estimations show that for values of $\gamma_{GB} - 2\gamma_{SL}$ in the order of magnitude of 100 mJ/m^2 the surface energy term in equation (12) dominates over the coherency strain term. However, for small values of $\gamma_{GB} - 2\gamma_{SL}$ in the order of magnitude of 1 mJ/m^2 the coherency strain term can be decisive. The value of $\gamma_{GB} - 2\gamma_{SL}$ can be very small due to the effects of prewetting [18]. Now we have the key for the understanding of the unusual behaviour of Ga in Al: from all the metals with a melting point lower than that of Al only Ga and Zn have a considerable solubility in solid Al [13]. However, the parameter η is small (0.021) for the Al–Zn system in comparison with that for the Al–Ga system (0.056). Therefore, only for Ga in Al the coherency strains can play a significant role and speed up the penetration process.

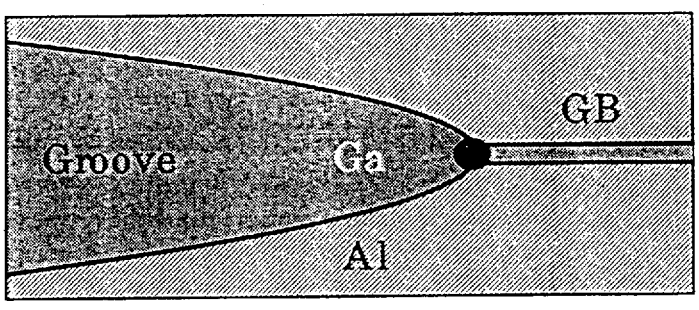

Fig. 7. The tip of the GB groove formed during the penetration of a liquid metal (Ga) along the GB in a solid matrix (Al).

CONCLUSIONS

From the results of present study the following conclusions can be drawn.

1. The dissolution of Fe–Si monocrystals in a Sn- or Zn-rich melt was found to occur in an unusual way: instead of a flat dissolution front and regular reduction of the monocrystalline sample in size a wide zone of pores filled with a melt is forming in the solid near the solid/liquid interface. The outer dimensions of the monocrystalline sample do not change during the experiment.
2. The observed inclusions are arranged in bands tilted with respect to the original solid/liquid interface on definite angles. Most probably, the inclusions are lying in (011) planes. The estimated bulk diffusional penetration length is much lower than the observed width of the zone with inclusions. Therefore, the phenomenon observed is different from the Liesegang phenomenon.
3. A model of the metal dissolution along the dislocation cores is proposed, in which the coherency strains in the bulk diffusion zone near the dislocations are taken into account. The model predicts that for energies of the solid/liquid interface below some critical value γ^*_{SL} the dislocation core is absolutely unstable against the dissolution in the melt. For the Fe–Sn system, $\gamma^*_{SL} \approx 203$ mJ/m^2. For higher values of the interfacial energy, the undersaturation of the bulk melt with the matrix metal is needed at the beginning of the dissolution process for the development of the instability.
4. Some other related phenomena are briefly considered, like the cracking of a solid metal in a melt and the rapid penetration of liquid metals along grain boundaries. The role of the coherency strains is underlined.

Acknowledgements—This work was partially supported by the Volkswagen Foundation under the grant I/69 000. Professors G. Purdy, L.S. Shvindlerman and R.A. Fournelle are greatly acknowledged for helpful discussions.

REFERENCES

[1] W.-H. Rhee and D.N. Yoon, *Acta metall.* **35**, 1447 (1987).
[2] M. Hillert, *Scripta metall.* **17**, 273 (1983).
[3] B.J. Spencer, P.W. Voorhees, S.H. Davis and G.B. McFadden, *The Effect of Compositionally-generated Elastic Stresses on Morphological Instability During Directional Solidification*, Technical Report, Northwestern University, Evanston, IL (1991).
[4] J.S. Kirkaldy and D.J. Young, *Diffusion in the Condensed State*, The Institute of Metals, London (1987), p. 416.
[5] C. Wagner, *J. Colloid Sci.* **5**, 85 (1950).
[6] E.I. Rabkin, V.N. Semenov, L.S. Shvindlerman and B.B. Straumal, *Acta metall. mater.* **39**, 627 (1991).
[7] E. Rabkin, B. Straumal, V. Semenov, W. Gust and B. Predel, *Acta metall. mater.* **43**, (1995), in press.
[8] R.L. Klueh and W.W. Mullins, *Acta metall.* **17**, 59 (1969).
[9] F.C. Frank, *Acta crystall.* **4**, 497 (1951).
[10] W. Missol, *Energy of Interfaces in Metals*, Slask, Katowice (1978), pp. 108 and 120.
[11] F.C. Larché, *Solid State Phenomena* **35-36**, 173 (1994).
[12] F.C. Larché and J.W. Cahn, *Acta metall. mater.* **33**, 331 (1985).
[13] T.B. Massalski et al. (eds.), *Binary Alloy Phase Diagrams*, ASM International, Materials Park, Ohio (1990), p. 1775; W.B. Pearson, *A Handbook of Lattice Spacings and Structures of Metals and Alloys*, Pergamon Press, Oxford (1967), p. 633; C.J. Smithells (ed.), *Metals Reference Book*, Butterworth, London (1976), p. 975.
[14] D.J. Srolovitz and S.A. Safran, *Phil. Mag. A* **52**, 793 (1985).

[15] I. Kaur, Y. Mishin and W. Gust, *Fundamentals of Grain and Interphase Boundary Diffusion*, John Wiley, Chichester (1995), p. 232.
[16] S.F. Pugh, *An Introduction to Grain Boundary Fracture in Metals*, The Institute of Metals, London (1991), p. 140.
[17] V.E. Fradkov, *Scripta metall. mater.* **30**, 1599 (1994).
[18] E.I. Rabkin, L.S. Shvindlerman, B.B. Straumal and W. Gust, *Mater. Sci. Forum* **126–128**, 305 (1993).

APPENDIX

The partial differential equation for the displacement field **u** in an isotropic solid is

$$(1-\nu)grad(div\mathbf{u})-\frac{1}{2}(1-2\nu)rot(rot\mathbf{u})-\eta(1+\nu)grad(c)=0 \tag{A1}$$

In cylindrical coordinates (r, ϕ, z) under the assumption of a cylindrical symmetry of **u**

$$\frac{\partial}{\partial r}\left(\frac{1}{r}\frac{\partial(ru)}{\partial r}\right)=\eta\frac{1+\nu}{1-\nu}\left(\frac{\partial c}{\partial r}\right) \tag{A2}$$

The solution of this equation which is finite for $r\rightarrow\infty$ is:

$$u(r)=\eta\frac{1+\nu}{1-\nu}\frac{1}{r}\int_{R}^{r}\xi c(\xi)d\xi+\frac{B}{r} \tag{A3}$$

where B=const. This constant can be determined from the condition $\sigma_{rr}(r=R)=0$. For the calculation of σ_{rr} the Hooke's law should be used:

$$\sigma_{rr}=\frac{E}{(1+\nu)(1-2\nu)}\left[(1-\nu)(u_{rr}-\eta c)+\nu\left(u_{\phi\phi}+u_{zz}-2\eta c\right)\right] \tag{A4}$$

where for a cylindrical symmetry $u_{rr}=\frac{\partial u}{\partial r}$, $u_{\phi\phi}=\frac{u}{r}$ and $u_{zz}=0$. Substituting (A3) into (A4) we find that B=0. For r=R one will have the following expressions for the deformations:

$$u_{rr}=\eta\frac{1+\nu}{1-\nu}c(R)$$
$$u_{\phi\phi}=0,\ u_{zz}=0 \tag{A5}$$

Here the solid without the solute atoms is considered as the reference state. It follows from the equations (A5) that the considered problem is equivalent to the problem of coherently strained half-space. Therefore, the elastic energy density

$$E_{coh} = \frac{E\eta^2 c^2}{1-\nu} \tag{A6}$$

Note, however, that equation (A6) is valid only for $r=R$. For $r>R$ the integrals like that from equation (A3) will be incorporated into the expression for the coherency strain energy, which makes the problem different from the case of a coherently strained half-space.